Phys.Rev.Lett., accepted

Supported magnetic nanoclusters: Softlanding of Pd clusters on a MgO surface

M. Moseler[1], H. Häkkinen[2] and U. Landman[2]
[1] *Theoretical Quantum Dynamics, Faculty of Physics, University of Freiburg, D-79104 Freiburg, Germany*
[2] *School of Physics, Georgia Institute of Technology, Atlanta, GA 30332-0430*

(February 1, 2008)

Low-energy deposition of neutral Pd_N clusters (N=2−7 and 13) on a MgO(001) surface F-center (FC) was studied by spin-density-functional molecular dynamics simulations. The incident clusters are steered by an attractive "funnel" created by the FC, resulting in adsorption of the cluster, with one of its atoms bonded atop of the FC. The deposited Pd_2-Pd_6 clusters retain their gas-phase structures, while for N>6 surface-commensurate isomers are energetically more favorable. Adsorbed clusters with $N > 3$ are found to remain magnetic at the surface.

PACS: 68.47.Jn, 68.43.Bc, 75.70.-i

Deposition of atomic clusters onto solid surfaces is a versatile surface-processing tool, with applications ranging from "micro-machining" and surface-smoothing to thin-film growth and fabrication of model nanocatalysts [1–7]. Theoretical investigations, employing most often molecular dynamics (MD) simulations in conjunction with semi-empirical classical interatomic potentials, guided many of the above experiments and provided valuable insights into the microscopic mechanisms of the deposition process [8–10]. However, in cases where the dominant part of the cluster-surface interaction involves surface chemistry (that is, the creation or breaking of chemical bonds) [7], spin-dependent (magnetic) processes [2], or surface defects of electronic origin (such as a F-center on an ionic surface) [3,11,12], a full quantum description of the cluster deposition process is necessary.

Here we report on a first-principles investigation of softlanding of Pd_N clusters (N=2-7 and 13) onto a MgO(001) surface containing a surface F-center, FC (oxygen vacancy), yielding microscopic details about the cluster adsorption mechanism and the evolution of the atomic, electronic, and spin degrees of freedom during the process. We show that the interaction between the Pd cluster and the FC evolves from an initial long-ranged attractive polarization into chemical bonding involving the localized FC electronic state located in the MgO band gap. A common structural motif for the adsorption geometry of the smaller clusters (N≤6) is found where the cluster retains its gas-phase geometry, whereas the larger clusters (N=7 and 13) adapt upon adsorption to the underlying surface rocksalt structure. The interaction with the surface quenches the spin for clusters with N≤3, retains the gas-phase triplet state (S=1) for $4 \leq N \leq 7$, and for N=13 the gas-phase nonet (S=4) transforms to a septet (S=3) state. These results are of importance for understanding the activity of Pd/MgO nanocatalysts [13,14], as well as for future investigations of supported magnetic clusters and nanoparticles.

The Pd_N/MgO system was treated within the framework of the local-spin-density functional (LSD) theory, with norm-conserving scalar-relativistic pseudopotentials [15] and self-consistent gradient corrections (PBE-GGA) [16]. For cluster impact energies below the band gap of the substrate material, the Born-Oppenheimer (BO) approximation provides a faithful description of the collision dynamics and therefore we employed the BO-LSD-MD method [17] for the calculation of the electronic structure and the nuclear motion of the Pd cluster and the substrate. The MgO substrate with the F-center was modeled with a two-layer *ab-initio* cluster $Mg_{13}O_{12}$, embedded into a lattice of point-charges in order to simulate the long-range Madelung potential [13]. The lattice parameter of the embedding part of the substrate was fixed to the experimental value (4.21 Å) of bulk MgO. The Pd_N cluster and the F-center's 4 nearest-neighbor Mg atoms and 4 nearest-neighbor O atoms of the first layer were treated dynamically during the deposition. To model the heat conductivity of the extended MgO surface the equations of motion of the dynamic surface atoms included an added damping term with a damping constant $\pi\omega_D/6$ [10], where ω_D is the Debye frequency of bulk MgO.

The initial spin states (triplet for N=2−7 and nonet for N=13) and geometrical structures of the Pd_N clusters were taken from our recent gas-phase study [18]. The clusters were placed with a random orientation 4 Å above the FC (measured from the cluster atom closest to the surface) and an initial velocity directed perpendicular to the MgO surface, corresponding to a kinetic energy of 0.1 eV per atom to simulate softlanding conditions. [19] The spin of the cluster-substrate system was dynamically evaluated at each MD time step. Subsequent to the dynamical evaluation of the deposition process for about 1 ps the simulation was stopped, and starting from the last recorded configuration a corresponding potential energy minimum was located by an energy-gradient optimization with variable spin; other spin-isomers (SPIs) were optimized (starting from the aforementioned optimal

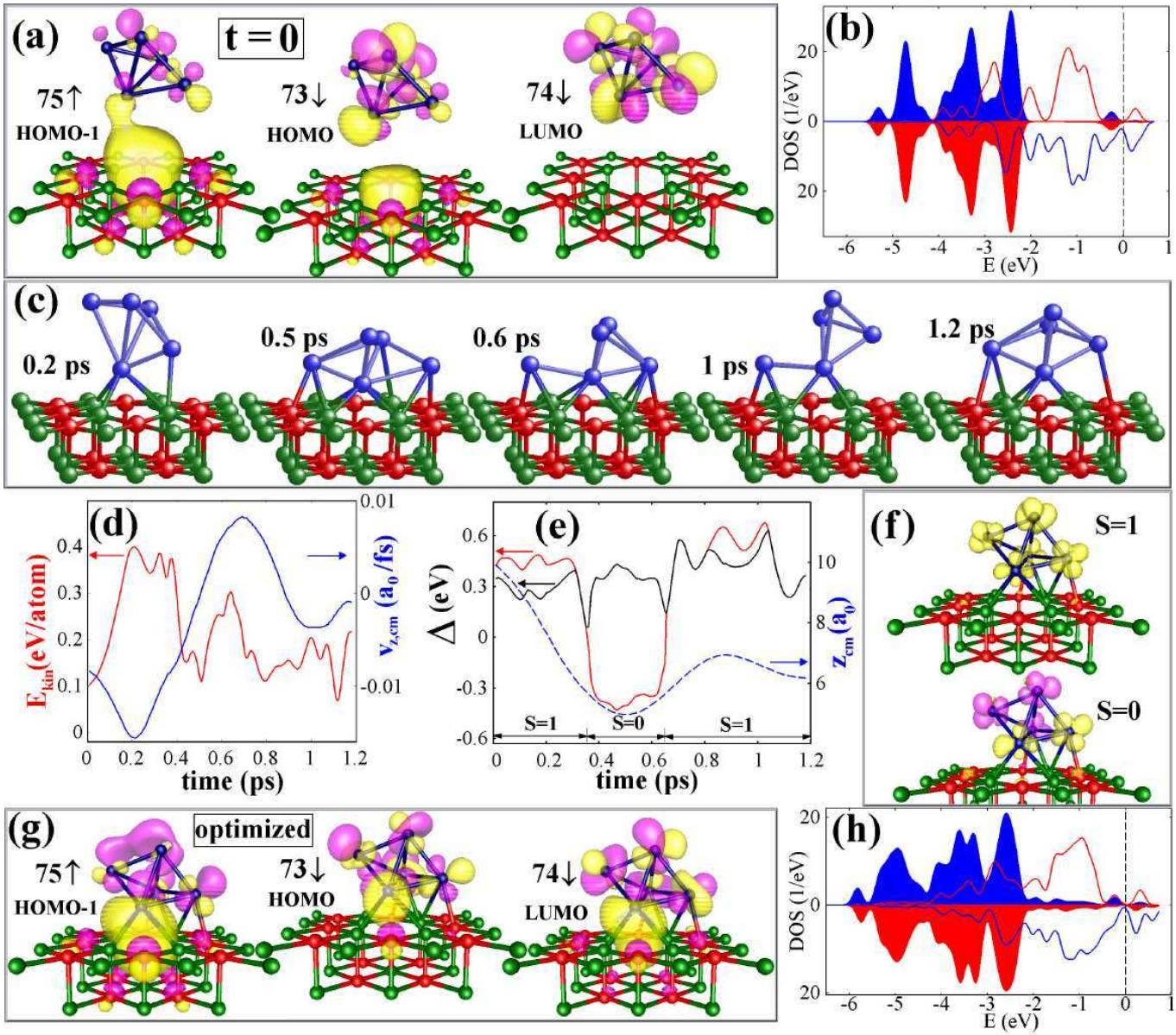

FIG. 1. A Pd_5 cluster impinges with 0.1 eV/atom kinetic energy on an F-center in a MgO (001) surface. Pd atoms are depicted as blue, Mg as green and O as red spheres. (a) Isosurfaces of the highest occupied up-spin molecular orbital (HOMO-1), the highest occupied down-spin orbital (HOMO) and the lowest unoccupied down-spin orbital (LUMO) of the initial configuration at t=0 (color coding distinguishes the sign of the wave function). Note, that the 75 up-spin and 73 down-spin orbitals are both occupied. (b) The corresponding local densities of states of the surface (blue area for up- and red area for the down-spin DOS) and of the cluster (red line for up- and blue line for down-spin DOS). The Fermi level, $E_F = 0$. We note that the DOS of the isolated surface and free cluster are essentially identical to that shown here, except for the first peak below E_F that corresponds to the long-range interaction discussed in the text. (c) Snapshots from the MD simulation recorded at the indicated times. (d) Time-evolution of the kinetic energy (red line) and the z-component of the CM velocity (blue line) of the cluster. (e) Evolution of the HOMO-LUMO gap (black line), of the eigenvalue energy difference $\epsilon_{74\downarrow} - \epsilon_{75\uparrow}$ (red line, see panel (a) for explanation of the orbital numbers), and of the z-component of the cluster's CM coordinate (blue dashed line). The triplet-singlet-triplet transition is indicated by the black arrows drawn on the time axis. (f) Isosurfaces of spin polarization density for the optimized triplet (S=1) and singlet (S=0) states. Yellow and purple denote excess of up and down spins, respectively. (g) Isosurfaces of the orbitals in (a) for the optimized adsorbed cluster. (h) The local DOS corresponding to the optimized cluster (color coding as in (b)).

configuration), in order to explore the thermal stability of the lowest-energy SPI.

The adsorption of a single Pd atom on top of the FC (tFC site) is characterized by a strong binding energy (3.31 eV) and a short equilibrium adsorption distance (1.65 Å), compared to adsorption on-top of an oxygen

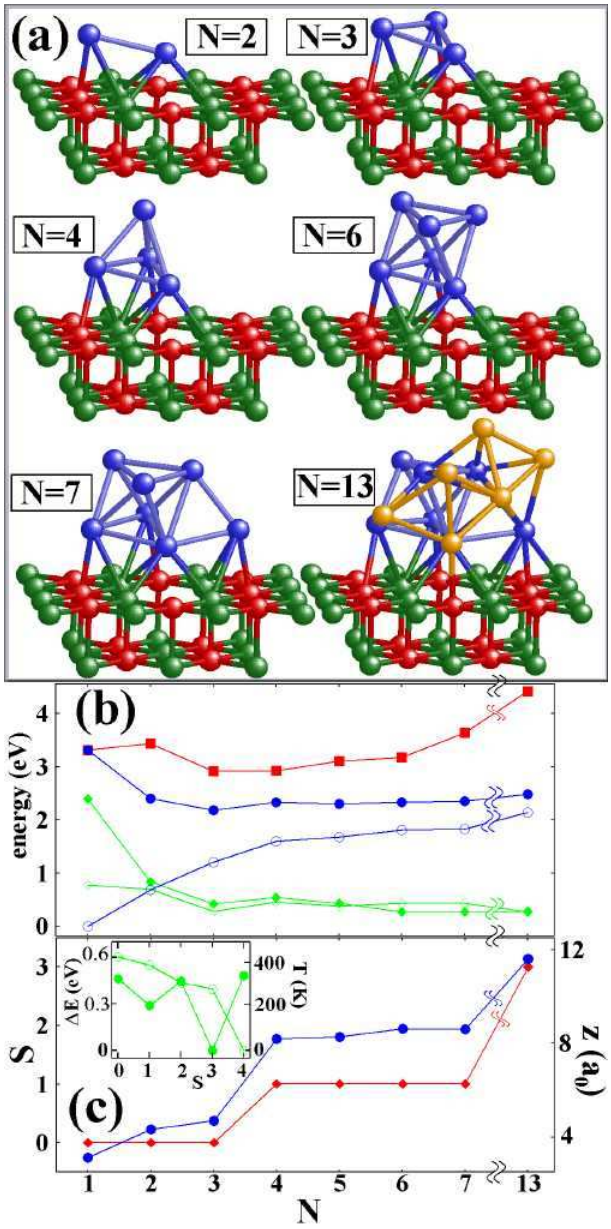

FIG. 2. Structural and magnetic size-evolution of supported Pd_N clusters. (a) GS structures of Pd_N (N=2,3,4,6,7 and 13). Color coding as in Fig. 1 except for Pd_{13} where a subset of the Pd atoms is colored in yellow in order to highlight the Pd_7 subunit (blue). (b) Size-evolution of the adhesion energy E_{ad} (red filled squares), the binding energy per atom E_b for the supported (blue solid dots) and free (blue circles) clusters, and the HOMO-LUMO gap of the supported (green solid diamonds) and free (green open diamonds) clusters. (c) Size evolution of GS spin S (red diamonds) and the distance of the highest cluster atom to the surface (blue solid dots). The inset in (c) shows the SPI energies ΔE (with reference to the GS configuration, $S = 3$ for the adsorbed cluster and $S = 4$ for the free one) and corresponding activation temperatures $T = 2\Delta E/k/(3N - 6)$, of supported (green solid dots) and free Pd_{13} (green circles) clusters.

(tO) atom at the ideal MgO surface (1.16 eV and 2.17 Å). The bonding between the Pd atom and the FC involves the localized FC electronic orbital, located in the band gap of MgO (separated from the top of the valence band by 2.3 eV), and (mainly) the $d(m = 0)$ orbital of the Pd atom. The attractive interaction to the F-center is rather long-ranged extending up to about 5 Å above the surface; e.g., the interaction energy of a Pd atom placed 5.2 Å above the FC is 0.1 eV. This weak attraction is due to polarization of the d(m=0) valence orbital of Pd by the FC. Surprisingly, we found that none of the other adsorption sites for the Pd atom, lying in the vicinity of the F-center (e.g., on-top of the neighboring oxygen (tO), on-top of the neighboring Mg atom (tMg), the Mg-Mg bridge (bMgMg), the Mg-O bridge (bMgO) and the Mg-Mg-O hollow site (hMgMgO)), are stable; i.e., optimization starting from any of these sites leads to a spontaneous (barrierless) transition to the aforementioned tFC configuration. We conclude that the F-center acts as a rather wide attractive "funnel" for the Pd atom, extending several Å both laterally and vertically [20]. This funneling effect steers the incident cluster and dominates the dynamics of the initial phases of the deposition process, as illustrated in the following for the representative case of a Pd_5 cluster.

When the Pd_5 cluster is placed 4 Å above the oxygen vacancy, the FC electronic state (located just below E_F) combines with d-orbitals of the closest Pd atom to form two bonding molecular orbitals (see the up-spin HOMO-1 and the down-spin HOMO in Fig. 1a). All other orbitals (for example the lowest unoccupied orbital (LUMO) of Pd_5 shown in Fig. 1a) remain to a large degree eigenstates of the separated systems, and consequently the corresponding density of states (DOS in Fig. 1b) may be represented as a superposition of those of the bare surface and the gas-phase cluster.

The long-range attraction between the cluster and the FC accelerates the lowermost Pd atom towards the tFC site (note the strong deformation of the Pd_5 cluster at 0.2 ps in Fig. 1c and the increase of the kinetic energy in Fig. 1d). Subsequently, other Pd atoms are attracted to neighboring bMgO positions (Fig. 1c, t=0.5 ps) accompanied by additional release of kinetic energy. Consequently, the center of mass (CM) velocity toward the surface increases to almost twice its initial value (Fig. 1d) leading to a strong flattening of the cluster at t=0.5 ps (see the minimum in the z component of the cluster CM in Fig. 1e). The cluster shape deformation causes a transient reordering of the molecular orbitals, i.e. it raises the energy of the up-spin HOMO-1 level (marked 75↑ in Fig. 1a) and turns it into a HOMO at t=0.32 ps, and even into a LUMO state at t=0.36 ps; this sequence is portrayed in Fig. 1e by closing of the HOMO-LUMO gap (black curve) and the minimum in the eigenvalue energy difference $\epsilon_{75\uparrow} - \epsilon_{74\downarrow}$ (red curve). Since the down-spin LUMO (74↓ in Fig. 1a) temporarily becomes the HOMO state, the total spin flips for a short time period

from S=1 to S=0 (Fig. 1e). After 0.5 ps the cluster recoils the reverse process drives the cluster back into the triplet spin state at t=0.63 ps (Fig. 1e).

Optimization of the adsorbed cluster after a 1.2 ps MD simulation (see Fig. 1c for the last MD configuration), resulted in a trigonal bipyramide structure (which coincides with the gas-phase optimal configuration) lying with a triangular facet against a *t*FC-*b*MgO-*b*MgO surface triangle (Fig. 1f). The spin polarization of the triplet ground state (see $S = 1$ isosurface in Fig. 1f) resembles that of the free cluster with a minor additional contribution from four surface oxygen atoms closest to the FC. As expected from our gas-phase calculations [18] the slightly higher-lying singlet state (ΔE=24 meV) consists of an anti-ferromagnetic ordering of the local magnetic moments (see $S = 0$ isosurface in Fig. 1f). The spatial character of the orbitals close to E_F and the surface and cluster contributions to the DOS of the triplet ground-state of Pd_5/MgO(FC) are shown in Figs. 1g and 1h, respectively.

Using the above-mentioned methodology, we have determined the ground-states for the other deposited Pd_N clusters [21]. For $3 \leq N \leq 6$ we observed a regular structural size evolution (Fig. 2a) where the gas-phase GS structures are anchored to the MgO surface with one Pd atom on the *t*FC, another Pd on *h*MgMgO site (for $N = 2$) or 2 additional Pd atoms on *b*MgO sites close to the *t*O position (for $3 \leq N \leq 6$). However, for Pd_7 and Pd_{13} the free clusters transform to structures that exhibit a higher degree of commensurability with the underlying surface, incorporating a Pd_6 and Pd_7 subunit, respectively (Fig. 2a). In this case, the loss in the intracluster cohesion is counterbalanced by a considerable gain of adhesion energy E_{ad} [defined as $E_{ad} = E(\mathrm{MgO(FC)}) + E(\mathrm{Pd}_N) - E(\mathrm{Pd}_N/\mathrm{MgO(FC)})$, see the red curve in Fig. 2b]. Consequently, the cohesive energy E_c per Pd atom [defined as $E_c = (E(\mathrm{MgO(FC)}) + NE(\mathrm{Pd}) - E(\mathrm{Pd}_N/\mathrm{MgO(FC)}))/N$, see the blue curve in Fig. 2b] continues to increase after Pd_6 and remains well above the gas-phase E_c values.

The HOMO-LUMO gap (Fig. 2b) of the combined Pd_N/MgO(FC) system is governed mainly by the metal cluster since the top part of its density of states lies in the MgO band gap. Most interestingly, the deposited Pd_N clusters with $N \geq 4$ remain magnetic: S=1 for $4 \leq N \leq 7$ and S=3 for N=13. The crossover from nonmagnetic to magnetic states between Pd_3 and Pd_4 correlates with an increased "thickness" of the cluster (Fig. 2c), corroborating our finding that flattening of the cluster on the surface tends to be accompanied by quenching of the spin (see discussion in the context of Fig. 1e).

In general, the deposition of the cluster reduces the energy separation between SPIs, thus lowering the threshold temperature for their coexistence. For instance, the triplet-singlet energy difference of supported Pd_4 is ΔE =65 meV compared to the gas-phase values of ΔE =136 meV; for Pd_{13} five SPIs can be found within a 0.5 eV range, which expressed in terms of temperature corresponds to about 350 K (fig. 2c, inset). This result indicates that experiments aiming at distinguishing magnetic states of the adsorbed clusters could be carried out at room temperature.

In summary, we have used first-principles simulations in studies of the dynamics of soft-landing of Pd clusters on a MgO(100) surface containing an F-center defect, and for explorations of the structural and spin characteristics of the adsorbed clusters. The F-center creates an attractive "funnel" for the approaching metal cluster, resulting in preferred binding configurations with one Pd atom atop the F-center. A common structural motif was found for the smaller adsorbed clusters (Pd_2 - Pd_6), where the cluster retains its gas-phase geometry. On the other hand, Pd_7 and Pd_{13} adapt upon adsorption to the underlying MgO rocksalt structure. Although the surface tends to reduce the spin of the adsorbed cluster, clusters larger than Pd_3 remain magnetic at the surface, exhibiting several low-lying structural and spin isomers. These results provide the impetus for further investigations regarding the interplay of structural and spin fluxionality of supported metal clusters and their catalytic properties, and call for an experimental verification of the predicted magnetic states of supported Pd clusters.

This research is supported by the U.S. AFOSR and the U.S. DOE (UL and HH), the "Deutsche Forschungsgemeinschaft" (MM), and the Academy of Finland (HH). Simulations were performed at the NIC (Jülich), HLRS (Stuttgart) and NERSC (Berkeley) computing centers.

[1] *Metal Clusters at Surfaces*, edited by K.H.Meiwes-Broer (Springer, Berlin, 2000).
[2] F.Parent et al., Phys. Rev. B **55**, 3683 (1997).
[3] see U.Heiz and W-D.Schneider, in ref. [1].
[4] O.Rattunde et al., J. Appl. Phys. **90**, 3226 (2001).
[5] R.Schaub et. al., Phys. Rev. Lett. **86**, 3590 (2001).
[6] C.Brechignac et al., Phys. Rev. Lett. **88**, 196103 (2002).
[7] J.Gspann, Surf. Rev. Lett. **3** 897 (1996).
[8] C.L.Cleveland and U.Landman, Science **257**, 355 (1992).
[9] H.P.Cheng and U.Landman, Science **260**, 1304 (1993).
[10] H.Haberland et al., Phys. Rev. B, **51**, 11061 (1995).
[11] H.Häkkinen and M.Manninen, J. Chem. Phys. **105**, 10565 (1996).
[12] L. Giordano et al., Phys. Rev. B, **64**, 075417 (2001).
[13] S. Abbet et al., Phys. Rev. Lett, **86**, 5950 (2001).
[14] S.Abbet et. al., J. Am. Chem. Soc. **122**, 3453 (2000).
[15] N.Troullier, and J.L.Martins, Phys. Rev. B **43**, 1993 (1991). The core radii (in a_0) are: Pd s(2.45) local, p(2.6), d(2.45); Mg s(2.5), p(2.75) local; O s(1.45), p(1.45) local. A plane-wave basis with a 62 Ry cutoff was used.
[16] J.P.Perdew et al., Phys. Rev. Lett. 77, 3865 (1996).

[17] R.Barnett and U.Landman, Phys. Rev. B **48**, 2081 (1993).

[18] M.Moseler et al., Phys. Rev. Lett, **86**, 2545 (2001). The optimal gas-phase geometries of the Pd_N clusters are as follows: $N = 3$, equilateral triangle; $N = 4$, tetrahedron; $N = 5$, trigonal bipyramide; $N = 6$, octahedron; $N = 7$, pentagonal bipyramide; $N = 13$, icosahedron.

[19] Since the first-principles simulations are rather computationally demanding, we have limited ourselves in most cases to only a few (uncorrelated) initial starting configurations, characterized by cluster orientations which are random with respect to the underlying surface structure. In all cases the final optimized configuration of the deposited cluster did not depend on the starting configuration, indicating the dominant influence of the attractive "funnel" effect due to the FC, as discussed in the text.

[20] Our study is relevant to a series of experiments [3] where nanocatalysts are prepared by softlanding metal clusters on thin MgO films containing typically a few % ML coverage of FCs. In this case, an average FC-FC distance is a few lattice constants. Therefore, most metal clusters either experience directly the "funnel effect" of the nearest FCs while approaching the MgO surface, or become trapped at FCs after a rather short surface diffusion path.

[21] In addition to the GS configurations we have examined for each of the Pd_N clusters, with $N \leq 7$, other structural/spin isomers which were optimized (to a local minimum) starting from several physically motivated chosen structures; in all cases (except Pd_6) this procedure resulted in isomers with higher energy compared to the structures determined via the dynamical deposition process. These higher-energy isomers include (the energy difference to the GS is given in parenthesis): a Pd_2 on *t*FC and *t*Mg (ΔE=0.33 eV), a Pd_4 tetrahedron on *t*FC-*t*Mg-*t*Mg (ΔE=0.41 eV), two rhombi on *t*FC-*b*MgO-*b*MgO-*t*O (ΔE=0.68 eV) and *t*FC-*t*Mg-*t*Mg-*b*MgMg (ΔE=0.84 eV), a Pd_5 square pyramide on *t*FC-*b*MgO-*b*MgO (ΔE=0.39 eV) and a Pd_7 PBP with one face on *t*FC-*b*MgO-*b*MgO (ΔE=0.45 eV). Pd_6 was the only case where the deposition dynamics ended in an isomer whose energy is higher than the GS structure (shown in Fig. 2(a)); the structure of this isomer is a distorted square pyramid on *t*FC-*b*MgO-*b*MgO and the sixth Pd atom is located at a *t*O position (ΔE=0.18 eV).